11 Computer Assisted Physics

C. Bersier, T. Mayer, P. F. Meier, E. Olbrich, S. Renold, and E. Stoll
guests: T. A. Claxton and H. U. Suter

In this report, we want to concentrate on the following research topics:

- Interpretation of the properties of high temperature superconductivity materials using spin-polarized *ab initio* calculations. The aim of this work is to provide insight into the particular microscopic electronic structure of cuprates.
- Non-linear dynamical study with particular reference to time series analysis of electroencephalograms in collaboration with two groups of the Medical Faculty.

We selectively report on the charge distribution in La_2CuO_4 before doping (11.1.1), muon sites and hyperfine fields in La_2CuO_4 and $Sr_2CuCl_2O_2$ (11.1.2), on the calculation of magnetic hyperfine coupling constants (11.1.3), and on results of time series analysis of sleep EEG (11.2).

11.1 Electronic structure of high-T_c materials

11.1.1 On the distribution of intrinsic holes in cuprates

La_2CuO_4 is insulating but becomes metallic and superconducting upon replacing a few percent of La^{3+} by Sr^{2+} or Ba^{2+}. The simplistic ionic model for the pure substance relies on the ions Cu^{2+}, O^{2-} and La^{3+}, the only hole in the electronic configuration being localized on Cu^{2+} in the $3d^9$ atomic configuration. The same assignment is made for the copper in the CuO_2 planes in $YBa_2Cu_3O_6$, the parent compound of the yttrium high-T_c family. To investigate the validity of this model we have performed first principles density functional calculations on the La_2CuO_4 crystal, simulated by using the Cu_5O_{26}/Cu_8La_{34} cluster (a picture of a similar cluster can be found in the next subsection) and have analyzed the charge distribution in detail.

There are 5 Cu atoms and 26 oxygen atoms in the cluster but for our discussion we select only those atoms at the center of the cluster for consideration. Those atoms close to the periphery of the cluster are not accounted for since these will include effects expected from the cluster edge. This cluster has five unpaired electrons leading to a choice of possible multiplicities, M = 2, 4 or 6. (M=6 corresponds to a "ferromagnetic" alignment of the spins, whereas M=4 leads to an "antiferromagnetic" alignment.) We list in Table 11.1 the total atom charges for the *central* copper and neighboring oxygen atoms in La_2CuO_4 which, in the present report, are for simplicity determined as averages of the charges resulting from multiplicities M=4 and M=6. A more detailed analysis may be found in Ref. [1].

Table 11.1: *Mulliken charges for Cu and for O_p and O_a, the planar and apical oxygens, respectively, for La_2CuO_4.*

Cu	O_p	O_a
1.16	-1.64	-1.94

Table 11.2: *Partial Mulliken populations for Cu and for O_p and O_a, the planar and apical oxygens, respectively.*

Cu			O_p		O_a
4s	$3d_{3z^2-r^2}$	$3d_{x^2-y^2}$	2s	$2p_{\|}$	$2p_z$
0.49	1.92	1.40	1.96	1.68	1.95

Furthermore, we present in Table 11.2 the corresponding Mulliken partial populations for those orbitals for which they deviate appreciably from the ionic picture.

The Mulliken charges in Table 11.1 suggest that 0.84 electrons are transferred to the oxygen atoms (Fig. 11.1). This result should be viewed with extreme caution if we continue to associate partial occupancy of orbitals with holes. For example using the Mulliken population data in Table 11.2 the hole is distributed 60% in the Cu $3d_{x^2-y^2}$ copper orbital, 9% in the $3d_{3z^2-r^2}$ copper orbital, 64% in the four planar oxygens $2p_{\|}$ orbitals (parallel to the bond) and 10% in the two apical oxygen $2p_z$ orbitals, which is clearly nonsense.

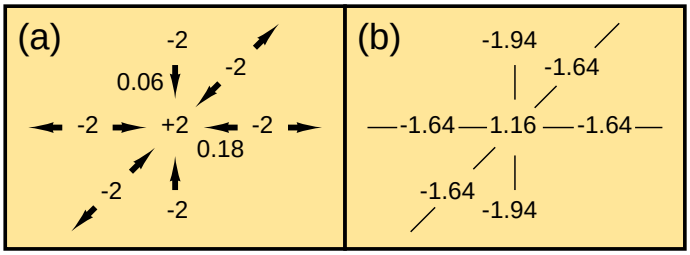

Figure 11.1: *(a) shows, using a simplistic model, the charge transfer of 0.84 electrons from oxygen anions (-2) to a copper cation (+2) as a result of covalent bonding. The charge transfers pointing away from the planar oxygen anions are to other planar copper cations which are not shown. Charges resulting from the hole transfer are given in (b).*

In order to proceed further we need to construct a molecular orbital energy diagram of the copper ion and its six nearest neighbor oxygen ions which leaves little room for doubt and explains the charge transfer observed. As is normal in similar circumstances we concentrate only on the frontier orbitals, the highest occupied, and for copper also at least the lowest unoccupied orbitals of the interacting ions. There is no difficulty with the Cu^{2+} ion since the qualitative orbital energy diagram has remained unchanged now for many years (see for example Ref. [2]) and is shown on the left hand side of Fig. 11.2 for O_h and D_{4h} symmetry. Note that we have added the copper $4s$ orbital, the unoccupied orbital of lowest energy .

In Table 11.2 only the four planar oxygen $2p_{\|}$ orbitals and the two apical oxygen $2p_z$ orbitals have significantly reduced populations from complete occupancy, which indicates that only these oxygen frontier orbitals are significantly involved in bonding. We define each of these $2p$ orbitals in such a way that the phases of the lobes pointing towards the central copper atom are the same. Fortunately in O_h symmetry we can form six symmetry adapted orbitals easily. Let the symmetry adapted orbitals be represented by Φ and the $2p$ orbitals by ϕ so that

$$\mathbf{\Phi} = \mathbf{U}\phi$$

where $\mathbf{U}$ is a unitary 6×6 matrix. The moduli of the non-zero elements of each row of the matrix are all identical and so we only require the sign of these elements. These are given in Fig. 11.3 for each Φ. The energies increase as a function of the number of nodal planes in each selection. Φ_1 has no nodal planes, $\Phi_2,\ \Phi_3,\ \Phi_4$ have one nodal plane and $\Phi_5,\ \Phi_6$ have two nodal planes. These are drawn on the extreme right of Fig. 11.2, that also shows, immediately to the left, how the degeneracies are lifted for D_{4h} symmetry. Only the $4s$ (a_{1g}) and $3d_{x^2-y^2}$ (b_{1g}) orbitals on the copper are available for bonding

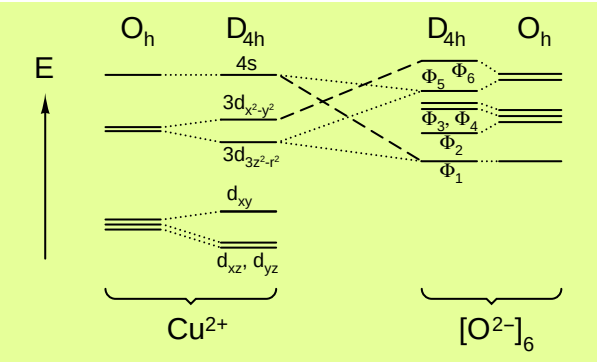

Figure 11.2: *Interaction of the atomic orbitals of copper with the symmetry combinations of the surrounding oxygen hybrid orbitals. The dashed lines indicate the primary interactions which remain even in O_h symmetry. The secondary (smaller) interactions are shown by dotted lines. Bonding and anti-bonding combinations of the orbitals of the primary interactions explain the occupancy of the 4s orbital and the transfer of the hole from the $3d_{x^2-y^2}$ orbital to oxygens (Φ_6 only).*

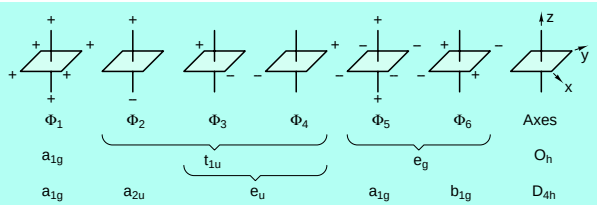

Figure 11.3: *The signs of the orbital coefficients for the various combinations of hybrid orbitals of the oxygen atoms. The absence of a sign indicates a zero coefficient. The hybrid orbitals are defined such that the phase pointing towards the copper atom have all the same sign.*

since these are not completely occupied. All the oxygen Φ orbitals are completely occupied and can only interact, if allowed by symmetry, by donating electrons into vacant or partially occupied orbitals on copper. The only interactions in O_h symmetry are $4s$–Φ_1 and $3d_{x^2-y^2}$–Φ_6. These are also allowed in D_{4h} symmetry and are regarded to be the dominant interactions. Secondary additional interactions arising from the reduction in symmetry to D_{4h} are $4s$–Φ_5, $3d_{3z^2-r^2}$–Φ_5 and $3d_{3z^2-r^2}$–Φ_1.

Since the hole, from the ionic model, originates from the $3d_{x^2-y^2}$ copper orbital there is *only one* interaction involving the hole: $3d_{x^2-y^2}$–Φ_6. This uniquely restricts the transfer from the copper to the planar oxygen $2p_\parallel$ orbitals (see definition of Φ_6 in Fig. 11.3). The Mulliken population analysis clearly indicates that 40% of the hole has been transferred to the planar oxygens (see Fig. 11.4 for more detail), and none, by this mechanism to the axial oxygens leaving 60% on the copper. Since a hole transfer is accompanied by an electron charge transfer in the opposite direction we conclude that of the 0.84 electrons transferred from the oxygens to copper, 0.40 electrons have been accounted for by the hole transfer. The remaining 0.44 electrons correspond almost exactly to the Mulliken $4s$ orbital population of 0.49 electrons which can be associated with the dominant $4s$–Φ_1 interaction. The discrepancy of 0.05 electrons can be attributed to the secondary interactions which also involve the $3d_{3z^2-r^2}$ orbital.

As concern spin densities we note that p_{spin}[Cu(4s)] = 0.03. This can be interpreted as arising from a spin polarization stemming from the unpaired electron in the $3d_{x^2-y^2}$-Φ_6 anti-bonding orbital, rather than a direct involvement in the hole transfer. However the effect on the hyperfine coupling constant is disproportionately large. The resultant spin in the $4s$ orbital polarizes the electrons in the $3s$ and to a minor extent in the $2s$ and $1s$ orbitals. The on-site contact hyperfine field is negative (-1.78 a_B^{-3}) but there exists a positive field that is transferred from nearest neighbor copper ions (+0.71 a_B^{-3}). A detailed analysis of these calculated spin transfers has been given in [3; 4]. Here, we first note that the theoretical results are in very good agreement with the values derived from the NMR data [5; 6]. We further note that Pavarini et al. [7] have emphasized the importance of the $4s$ orbital in intra layer hopping.

The hole distribution, which is predominantly centered on the $3d_{x^2-y^2}$ orbital on copper, should sensitively affect the EFG at the copper nucleus (see reference [3]) since this property is dependent

on the $1/r^3$ function.
The relatively high symmetry (D4h) of the immediate oxygen anion environment of copper cations, represented by the distorted octahedral cluster CuO_6^{10-} in La_2CuO_4, enables the hole distribution to be uniquely and unambiguously associated with the Cu $3d_{x^2-y^2}$ orbital and the symmetry adapted oxygen orbital Φ_6 from a qualitative molecular orbital energy diagram. The diagram also allows for the participation of the formerly unoccupied Cu $4s$ orbital in receiving electrons directly from two doubly occupied oxygen orbitals, without spin preference. It should now be clear that analysis of charge alone cannot determine the hole distribution. These results are in agreement with, and provide an explanation for, the Cu $4s$ orbital population from both previous band structure and current cluster calculations.

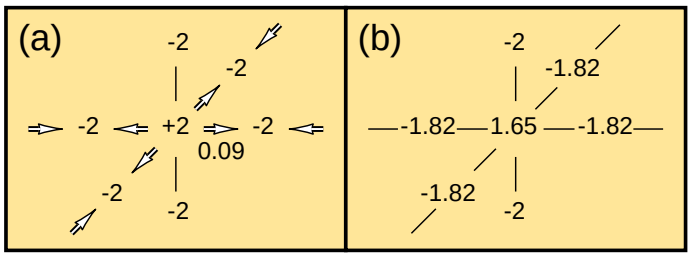

Figure 11.4: *(a) shows the transfer of 0.0875 holes from the copper cation to each of the planar oxygen anions arising from the bonding involving the Cu $3d_{x^2-y^2}$ orbital and the oxygen valence orbitals. The corresponding Mulliken charges resulting from the hole transfer is given in (b).*

11.1.2 Muon sites and hyperfine fields in La_2CuO_4 and $Sr_2CuCl_2O_2$

Positive muons are sensitive probes of local internal magnetic fields in solids and muon spin rotation (μSR) experiments have provided valuable insight into the microscopic nature of magnetism in a variety of substances, in particular also in cuprates. A disadvantage of the μSR method, however, is that the site in the crystallographic lattice at which the muon stops is not known. This is irrelevant for the study of the internal fields of flux line lattices where the distances between the flux cores are much larger than the dimension of the crystallographic unit cell. For the investigation of local magnetic fields in zero or small applied fields, however, a knowledge about the muon stopping site is necessary. Today, possible muon sites are estimated by comparing the measured local field with the dipolar field generated *in vacuo* by localized magnetic moments at the copper positions. The magnitude and directions of these moments are determined from neutron scattering data. The assumption that the local magnetic fields at muons result primarily from these remote moments, however still requires justification. We have therefore extended our cluster calculations on cuprates by inclusion of a muon at various sites and have determined the total energy allowing for lattice relaxation of neighboring atoms.

For the lanthanum compound La_2CuO_4 a small cluster, $\mu CuO_6/Cu_4La_{10}$, with only one copper atom in the core and a larger cluster, $\mu Cu_5O_{26}/Cu_8La_{34}$, which contains five copper atoms and is shown in Fig. 11.5 have been calculated. The smaller cluster was used to determine the relaxed geometry, whereas in the larger one the hyperfine parameters were calculated. The corresponding strontium clusters to simulate muons in $Sr_2CuCl_2O_2$ were also studied, namely $\mu CuO_4Cl_2/Cu_4Sr_{10}$ and $\mu Cu_5O_{16}Cl_{10}/Cu_8Sr_{34}$. The electronic structure calculation uses a hydrogen atom for the simulation of the muon, since the electronic wave function only depends on the charge and position of the atoms. Three muon sites were investigated. The first position, which is depicted in Fig. 11.5 and called site (A) is in the bond between the copper and the apical oxygen. Sites (B) and (C) which have been proposed before [8] are further away from the CuO_2 plane. The total energy, however, is lowest for site (A). The geometry optimisation resulted in pushing the Cu by 0.34 a_B (0.08) below the CuO_2 plane and moving the O upwards 0.43 a_B (0.52) (where the numbers in parentheses refer to $Sr_2CuCl_2O_2$).

Thus, contrary to the general belief, the bond centered position of the muon is preferred. A similar site has been attributed to the anomalous muonium in semiconductors. In the case of the lanthanum compound the muon is close to the appex oxygen atom, suggesting an $(O\mu)^-$ type species. From a chemical viewpoint one would interpret this configuration at this site as an $(OH)^-$ close to the Cu^{2+} ion. For the strontium compound this is not possible, therefore the muon is closer to the in–plane copper atom.
A comparison of the different geometries in the two materials shows that the calculated distance of the muon from the copper where the magnetic moments are centered, is larger in La_2CuO_4 than in $Sr_2CuO_2Cl_2$ by a factor of 1.21. Since both transferred and dipolar fields decrease with the third power of the distance, one expects from these geometries smaller fields in La_2CuO_4 than in $Sr_2CuO_2Cl_2$ by roughly a factor two. This compares favourably with the observed ratio of about three for the experimental hyperfine coupling constants of the two compounds and explains the larger frequencies found in the strontium compound.

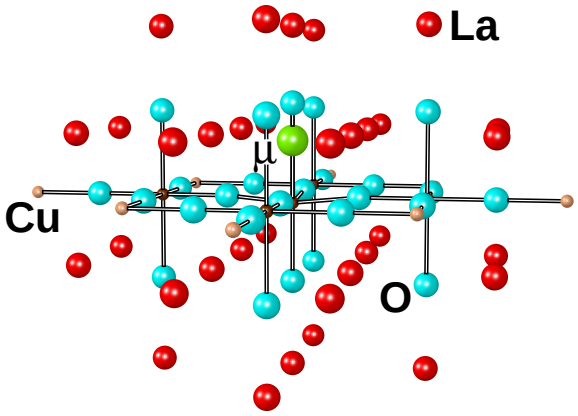

Figure 11.5: *The HCu_5O_{26}/Cu_8La_{34} cluster with the hydrogen (muon) at position A.*

We further note that the small mass of the muon implies a large spread of its quantum-mechanical ground-state wave function. This must be accounted for in more precise theoretical estimates of the spin densities at the muon.

In summary, the ab-initio cluster calculations show transferred hyperfine fields at muon sites in La_2CuO_4 which are in disagreement with the common interpretation of μSR experiments in cuprates. This is not completely surprising since a large amount of information about on–site and transferred hyperfine fields in cuprates is available: numerous nuclear magnetic resonance (NMR) experiments have been performed in the very same substances which were explored by μSR, yet it seems that the progress in understanding NMR data has so far been ignored by the μSR community.

11.1.3 Investigations into static NMR properties in cuprates

NMR measurements of the copper Knight shift in cuprates exhibit an amazing peculiarity. With the external magnetic field applied parallel to the CuO_2 planes the Knight shift declines in the superconducting state with decreasing temperature as is expected from the reduction in the spin susceptibility. With the field perpendicular to the planes, however, the shift is independent of the temperature in all compounds of the La- and Y- family irrespective of the doping level. This has been explained by an incidental cancellation of an on-site and a transferred hyperfine field at the copper nucleus. These quantities, however, depend on the lattice parameters and it is astonishing that the same coincidence should occur in both families.

Cluster calculations have the advantage that relative changes of magnetic hyperfine coupling constants (MHCC) upon changes in lattice parameters can be investigated. Therefore we have extended previous calculations of MHCC in La_2CuO_4 [9] and $YBa_2Cu_3O_7$ to include also $Sr_2CuO_2Cl_2$ and $YBa_2Cu_3O_6$.[10] Additional calculations have been performed in clusters with artificially stretched and squeezed planar lattice constant $a' = f \cdot a$ and $b' = f \cdot b$, with $f \in (0.99, 1.01)$. Furthermore, a La_2CuO_4 cluster was set up with an artifically buckled CuO_2 plane. In this way the behavior of the MHCCs under lattice distortions could be observed.

Selected results for the transferred hyperfine coupling, B, and the on-site dipolar interaction, $A^{\parallel}_{dip}$ at the planar copper nuclei are presented and plotted against the lattice constant in Figs. 11.6 and 11.7. As expected, the transferred hyperfine interaction drops in all compounds when increasing the lattice constant. However, in the yttrium based compounds, the transferred field is much smaller than in the other two compounds. Interestingly, B drops also upon an artificial buckling of the planes in the La compound as indicated by the red crosses.

The on-site dipolar interaction, $A^{\parallel}_{dip}$ gets also weaker when enlarging the unit cell and scales quite well with the lattice constant. It is seen that the buckling has only a minor effect on the dipolar interaction.

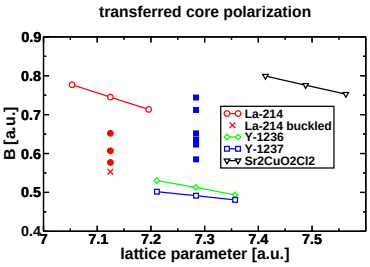

Figure 11.6: *Theoretical (open symbols) and experimental (closed symbols) values for the transferred copper hyperfine interaction (left panel) and for the on-site dipolar coupling (right panel) for various cuprates plotted against the lattice parameters.*

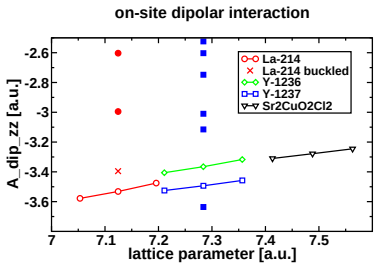

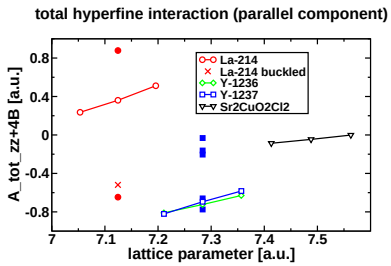

Figure 11.7: *Corresponding results for the total copper hyperfine interaction.*

As a conclusion, we think that the current explanation of a temperature independent Knight shift in c-direction may be in error. The proposal of a large residual shift at low temperatures could help in establishing a new understanding of the spin properties in cuprates.

In Fig. 11.7, the total hyperfine interaction along the c-axis is displayed. It is zero neither in the lanthanum compound nor in the yttrium compounds. The anisotropy of the total hyperfine interaction especially for $YBa_2Cu_3O_7$ ($[A^{\parallel}_{tot} + 4B]/[A^{\perp}_{tot} + 4B] \simeq 4$) shows that the non-zero hyperfine interaction should be observable in NMR experiments. Furthermore the buckling of the lanthanum compound drastically changes the total hyperfine interaction.

In conclusion, a cancellation of hyperfine fields for all cuprates cannot be corroborated by our calculations. The transferred interaction B has the largest influence on the anisotropy of the total hyperfine fields. Therefore, it seems reasonable to assume that - in a first approximation - the on-site hyperfine fields are essentially of the same size in all cuprates.

11.2 Time series analysis of EEG

Research on time series analysis of EEG data was centered on the further investigation of oscillatory events in the human sleep EEG. This research is conducted in close collaboration with the institute of pharmacology and toxicology.

Sleep oscillations, such as delta waves, K-complexes or sleep spindles are typical patterns in the sleep EEG, which are a main ingredient for the definition of sleep stages and might have an important function with regard to processes of synaptic plasticity during sleep, i.e. for learning and memory consolidation [11]. Therefore their detection, the characterization of their properties and appropriate models for their dynamics are important for a further understanding of their role in sleep.

Using a new algorithm for the detection of oscillatory events based on adaptive autoregressive modeling we studied the changes of their properties throughout the night. Fig. 11.8 shows an example of one night with the events denoted as dots at a particular time and frequency. In the lower panel the hypnogram, i.e. the sleep stages, are shown.

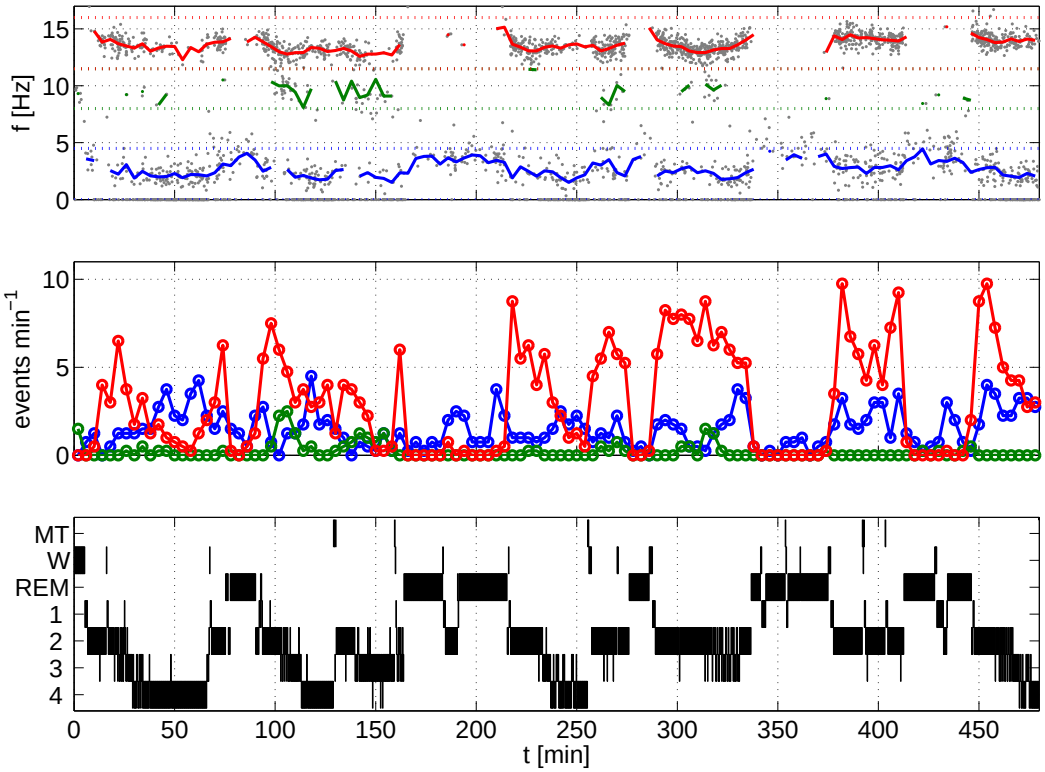

Figure 11.8: *Mean frequencies (top) and event densities (middle) of the oscillatory events for the three frequency bands for one night. The dotted lines in the upper panel denote the limits of the frequency bands. The grey points mark frequency and time for single events.*

We found that oscillatory events occurred essentially in three frequency bands: sigma (11.5-16 Hz, sleep spindles), alpha (8-11.5 Hz) and delta (0.75-4.5 Hz, delta waves and K-complexes). Their incidence showed only small intra- but large interindividual differences: the largest interindividual differences were found with respect to alpha events, we found individuals with a large amount of alpha events in sleep stages 3 and 4 (alpha-delta sleep), individuals with only a small amount of alpha events in REM sleep and sleep stage 1 and individuals with almost no alpha events at all.
The left panel of Fig. 11.9 illustrates the sleep stage dependencies of the mean event densities and their mean frequencies for the three types of events. The incidence of sleep spindles is maximal for sleep stage 2 and the incidence of delta events increases with the deepening of sleep. While this behavior is in agreement with standard knowledge the observed frequency behavior is less well known. The properties of the oscillatory events depend not only on the sleep stages but also on the time during the night, which can be studied by distinguishing the different REM-NREM cycles. See the hypnogram in Fig 11.8 for an example. This night shows five complete cycles. The right panel of Fig. 11.9 shows the results for sleep stage 2. The observed changes of the properties of oscillatory events during sleep are important for a deepening of our understanding of slow processes during sleep connected to synaptic plasticity.

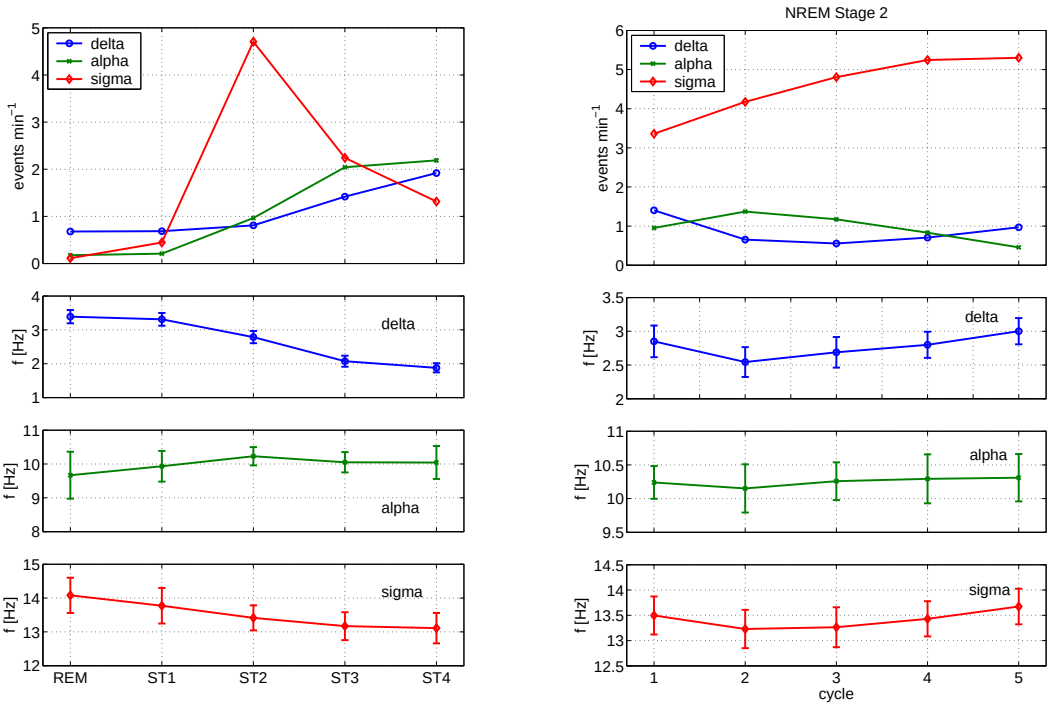

Figure 11.9: *Mean event densities (top) and mean frequencies (below) for the three frequency bands from a larger set of subjects and nights. The error bars denote the standard deviations with respect to the subjects. The left panel shows the sleep stage dependence and the right panel the influence of the sleep cycle, i.e. the time in the night.*

[1] E. P. Stoll, P. F. Meier, and T.A. Claxton, J. Phys.: Condens. Matter, **15**, 7881 (2003).

[2] H. H. Schmidtke in *Phys. Methods in Adv. Inorganic Chemistry*, edited by H. A. O. Hill and P. Day, Interscience London 1968, p. 107.

[3] E. P. Stoll, T. A. Claxton, and P. F. Meier, Phys.Rev.B **65**, 064532 (2002).

[4] P. F. Meier, T. A Claxton, P. Hüsser, S. Pliberšek, and E. P. Stoll, Z. Naturforschung **55 a**, 247 (2000).

[5] Y. Zha, V. Barzykin, and D. Pines, Phys.Rev.B **54**, 7561 (1996).

[6] T. Imai, J. Phys. Soc. Japan **59**, 2508 (1990).

[7] E. Pavarini, I. Dasgupta, T. Saha-Dasgupta, O. Jepsen, and O. K. Andersen, Phys.Rev.Lett.**87**, 047003 (2001).

[8] S. B. Sulaiman, N. Sahoo, T. P. Das, O. Donzelli, E. Torikai and K. Nagamine, Phys.Rev.B **44**, 7028 (1991).

[9] S. Renold and P. F. Meier, J. Supercond. Inc. Nov. Magn. **16**, 483 (2003).

[10] S. Renold, T. Heine, J. Weber, and P. F. Meier, Phys.Rev.B **67**, 024501 (2003).

[11] M. Steriade and I. Timofeev, Neuron review **37**, 563 (2003).